ELSEVIER

Contents lists available at ScienceDirect

Acta Biomaterialia

journal homepage: www.elsevier.com/locate/actbio



Full length article

Semaphorin 3A delivered by a rapidly polymerizing click hydrogel overcomes impaired implant osseointegration in a rat type 2 diabetes model



Jingyao Deng^{a,b}, David J. Cohen^a, Eleanor L. Sabalewski^a, Christine Van Duyn^a, D. Scott Wilson^c, Zvi Schwartz^{a,d}, Barbara D. Boyan^{a,e,*}

- ^a Department of Biomedical Engineering, College of Engineering, Virginia Commonwealth University, 601 West Main Street, Richmond, VA 23284, USA
- ^b VCU DaVinci Center for Innovation, Virginia Commonwealth University, Richmond, VA 23284, USA
- ^c Translational Tissue Engineering Center, Johns Hopkins University, Baltimore, MA 21231, USA
- ^d Department of Periodontics, University of Texas Health Science Center at San Antonio, San Antonio, TX 78229, USA
- e Wallace H. Coulter Department of Biomedical Engineering, Georgia Institute of Technology, Atlanta, GA 30332, USA

ARTICLE INFO

Article history: Received 21 July 2022 Revised 14 November 2022 Accepted 16 November 2022 Available online 24 November 2022

Keywords: Hydrogel Titanium Implants Type 2 diabetes Bone regeneration Semaphorin 3A Bone formation

ABSTRACT

Semaphorin 3A (sema3A) is an osteoprotective factor that enhances bone formation while inhibiting osteoclast bone resorption. It is produced by rat calvarial osteoblasts cultured on grit-blasted/acid-etched microtextured (SLA) titanium surfaces at higher levels than on tissue culture polystyrene, suggesting that it may improve performance of titanium implants in vivo, particularly in conditions characterized by compromised bone quality. To test this, we established a clinically relevant type 2 diabetes mellitus (T2DM) rat model and used a non-toxic click hydrogel that rapidly polymerizes in situ (GEL) to provide localized controlled delivery of sema3A. In vitro studies confirmed that sema3A released from GEL was biologically active, increasing osteoblast differentiation of a pre-osteoblast cell-line. Whereas increased sema3A production was not observed in T2DM calvarial osteoblasts cultured on SLA, exogenous sema3A enhanced surface-induced osteoblast differentiation, indicating that it would be a viable candidate for in vivo use. Delivery of sema3A either by GEL or by local injection to bone defects enhanced osseointegration of SLA implants in the T2DM rats. Trabecular bone mass and bone-to-implant contact were decreased in T2DM rats compared to normal rats; sema3A delivered locally improved both parameters. These findings suggest that reduced trabecular bone contributes to poor osseointegration in T2DM patients and support GEL as a promising treatment option for sustained release of therapeutic doses of sema3A. Moreover, using this clinically translatable T2DM model and developing a biocompatible, Cu-free click chemistry hydrogel platform for the non-invasive delivery of therapeutics has major implications for regenerative medicine as a whole.

Statement of significance

Osseointegration is compromised in patients with poor bone quality due to conditions like type 2 diabetes mellitus (T2DM). Previously, we showed that semaphorin 3A (sema3A) production is increased when human bone marrow stromal cells are cultured on titanium substrates that support osseointegration *in vivo*, suggesting it may enhance peri-implant osteogenesis in diabetes. Here we established a spontaneously developing T2DM rat model with clinical translatability and used it to assess sema3A effectiveness. Sema3A was delivered to the implant site via a novel copper-free click hydrogel, which has minimal swelling behavior and superior rheological properties. Osseointegration was successfully restored, and enhanced compared to burst release through injections. This study provides scientific evidence for using sema3A to treat impaired osseointegration in T2DM patients.

© 2022 Acta Materialia Inc. Published by Elsevier Ltd. All rights reserved.

E-mail address: bboyan@vcu.edu (B.D. Boyan).

^{*} Corresponding author at: Department of Biomedical Engineering, College of Engineering, Virginia Commonwealth University, 601 West Main Street, Richmond, VA 23284, USA

1. Introduction

Dental implants have enabled the restoration of dentition in the growing aging population, which has resulted in improved health for many individuals. However, poor bone quality associated with diseases like type 2 diabetes mellitus (T2DM) and osteoporosis impacts implant survival [1,2]. Even though some reports have indicated that the success rate of dental implants in diabetic patients is comparable to non-diabetic patients, current evidence supports the hypothesis that T2DM patients with a poorly or moderately controlled glycemic level have a higher early implant failure rate than well-controlled T2DM patients [3–9].

Implant success depends on osseointegration [10,11]. Our group has previously demonstrated that surface treatments that produce macro/micro/nano-textured features on titanium implants can enhance osseointegration [10,12,13]. A contributing factor to this is the production of osteogenic factors by bone marrow stromal cells (BMSCs) on the surface, including bone morphogenetic protein-2 (BMP2) and BMP4, as well as the downregulation of inflammatory mediators like interleukin 6 (IL6) [14–16].

Recently, we found that the production of the nerve-derived protein semaphorin 3A (sema3A) by BMSCs was sensitive to Ti surface properties, including microtopography and chemistry. Sema3A is a known osteoprotective factor that both increases bone formation and inhibits bone resorption [17-21]. It has been reported to promote osteoblast differentiation of BMSCs isolated from diabetic rats [22]. Furthermore, sema3A was shown to mitigate the inhibitory effect of high glucose on osteogenesis using a mouse osteoblast cell line in vitro [23]. These studies, together with our observations on the effects of sema3A on enhancing BMSC differentiation on microtextured titanium surfaces [24] suggested that sema3A might be a useful therapeutic for promoting peri-implant osteogenesis in T2DM in vivo. We hypothesized that localized delivery of sema3A at the site of implantation would be a more powerful therapeutic strategy to impact surrounding osteoblast-lineage cells, mobilizing them to enhance osseointegration under compromised conditions, such as T2DM.

One of the challenges when administering this potent factor as a potential therapeutic is delivering it at an adequate concentration within a sufficient therapeutic window to elicit the desired cellular effects and achieve a favorable outcome in compromised patients. Our strategy for achieving sustained delivery of sema3A was to use a minimally invasive, rapidly polymerizing, click chemistrybased hydrogel. Hydrogels are biomaterials composed of hydrated, crosslinked networks of water-soluble polymers that have been extensively employed as vehicles for drug encapsulation and sustained delivery of therapeutics. The bio-orthogonal, injectable hydrogel described in this study forms a stable gel in under 90 s at 37°C through a ring-strain promoted Cu-free click reaction between azide functionalized PEG polymers and a DBCO functionalized PEG crosslinker without external photo-initiators and without generating heat. The rapid encapsulation of bioactive molecules into the hydrogel maintains the biologics at the delivery site over an extended time. Ester linkages degrade in vivo and ultimately release the loaded molecules [25]. When biocompatibility of a similar click hydrogel was tested in critical size defects in the craniums of weanling and adult mice, degradation occurred over 5 to 10 days without releasing any toxic molecules or by-products. Histologically, there was no evidence of pathology in the surrounding tissues [25,26] suggesting that the current formulation would be an ideal platform for sema3A delivery.

In these studies, we employed the Zucker Diabetic Sprague Dawley (ZDSD) rats, a clinically relevant T2DM rodent model. Unlike the prevailing diabetic rodent models that are either induced by chemical toxin injection (such as streptozotocin or alloxan) [27,28] or via genetic mutations (leptin or leptin receptor defi-

ciency) [29], ZDSD rats develop T2DM spontaneously when fed a high fat diet. Thus, the ZDSD rat is a model that closely resembles factors contributing to the manifestation of T2DM in humans [30–32]. Using this model will allow clinicians to better translate findings to benefit the human condition and improve clinical outcomes when managing T2DM patients receiving implants.

The goal of this study was to determine if sema3A delivered locally via the click hydrogel could impact osteogenesis in a compromised bone model. The formulation selected for this initial study was shown to be effective for delivery of peptides, antibodies, and drugs in our previous studies, although the hydrogel characteristics can be modified to vary the concentration of factor within the gel, the gel degradation kinetics, and the kinetics of factor release. Here we report the impact of T2DM on the osseointegration of microtextured titanium implants in the ZDSD rat model and deliver sema3A in two modalities: via direct incorporation into the click hydrogel and via local injection of sema3A over the implant site. In addition, the effect of sustained delivery versus burst release of sema3A is demonstrated in this study. Finally, we assessed the effects of T2DM on the ability of rat calvarial osteoblasts to respond to the Ti surface *in vitro*.

2. Materials and methods

2.1. Hydrogel preparation

The methods for preparing our click hydrogel were described in previous studies [25,26]. Briefly, the rapidly polymerizing hydrogel was synthesized by mixing two aqueous solutions that undergo in situ chemical crosslinking via copper-free click-based chemistry. Dibenzocyclooctyne-functionalized poly-ethylene glycol (PEG) crosslinker (DBCO-functionalized PEG) was synthesized by Thiol-Michel addition reaction between PEG-dithiol and dibenzocyclooctyne maleimide (DBCO-maleimide). The DBCO-functionalized precursor forms an in-situ crosslinked hydrogel with azide functionalized acylate polymer. To generate a water-soluble non-fouling multivalent azide functionalized polymer, PEG-N3 was synthesized from azide functionalized and non-functionalized PEG methacrylate monomers via reversible addition-fragmentation chain transfer (RAFT) polymerization, which affords tight control of azide functionality. The components of the hydrogel were synthesized according to our specifications at a commercial facility (Syngene International, Bengaluru, India), and shipped lyophilized to our laboratory. The components were reconstituted in sterile 1X PBS (ThermoFisher Scientific, Waltham, MA, USA) and stored in -80°C before use. The hydrogel was formed by mixing one part of PEG-N3 (50%; w:v) and two parts of PEG-DBCO (12.5%; w:v) using a dual-syringe dispensing apparatus that dispenses the two solutions simultaneously at a 2:1 ratio.

2.2. Hydrogel characterization

To assess swelling, the surface areas were analyzed by ImageJ to determine the swelling ratio (q_t) , normalized to T_0 . The horizontal degree of swelling was defined by the average swelling ratio $(q_t) \pm$ the standard error (SEM), where the surface area of the hydrogel at each time point compared with its initial measurement is divided by the initial surface area. Vertical swelling was assessed by percent weight and volume change under physiological conditions at 37°C for 1h, 2h, 3h, 8h, 12h, 24h, and 48h.

To assess gelation, the viscosity-sensitive probe, 2-cyano-3-(2,3,6,7-tetrahydro-1H,5H-benzo[ij]quinolizin-9-yl)-2-propenoic acid (CCVJ) solution (Cayman Chemical, Ann Arbor, MI, USA) was loaded into the crosslinker solution and combined with the copolymer to form the click hydrogel, which was visualized by fluorescence microscopy (Zeiss AxioCam Observer Z1, Oberkochen,

Germany) at an emission of 497 nm for 5 mins. A conservative threshold intensity (>1000 A.U.) was determined by the glycerol standard. Total fluorescence was determined by the number of pixels above the threshold fluorescence intensity.

Rheological measurements (Rheology Testing Services, Chapel Hill, NC) were performed immediately upon hydrogel polymerization at 37°C. A Malvern Kinexus Pro Rheometer equipped with 25 mm roughened parallel plates and a gap height of 400 μ m (n=3) was used to characterize the rheological properties of the hydrogel. Hydrogels were allowed to cure at 37°C for 5 mins. The force required to separate the two plates vertically was measured (pull-away speed of 5 mm/s). Force displacement curves were generated to quantify the maximum force required to separate the two plates vertically (tackiness). Amplitude sweep experiments were conducted using increasing oscillatory strain at a constant frequency to determine the hydrogel's linear viscoelastic region (LVER). Frequency sweep experiments were made over a range of oscillation frequencies (0.1-20 Hz) at 37°C at a constant oscillation amplitude (0.5% strain)—a polydimethylsiloxane (PDMS) viscoelastic standard under the same parameters used for the hydrogel samples.

Proton nuclear magnetic resonance:

¹H NMR analysis was performed on a Bruker Avance III 600 MHz spectrometer. 50 to 100 mg of lyophilized copolymer and crosslinker were dissolved in approximately 0.85 mL of deuterated water (D2O) or deuterated chloroform (CDCl3). ¹H NMR chemical shifts were at 4.79 ppm for water and 7.26 for chloroform.

2.3. Sema3A release kinetics and in vitro bioactivity of sema3A released from the hydrogel

For our release studies, 6 μ g recombinant sema3A (R&D Systems) was loaded into the click hydrogel. The gels with or without sema3A were incubated at 37°C in 300 μ L of Dulbecco's modified Eagle medium (DMEM; Mediatech) and 1% penicillinstreptomycin (VWR International). DMEM were collected and replaced on days 1-5. Bio-Dot assay (Bio-Rad Laboratories) was used to quantify hydrogel-released sema3A, according to the manufacturer's instructions [33].

MG63 human osteoblast-like cells (ATCC) were cultured at 10,000 cells/cm² in a 24-well plate with DMEM with 10% fetal bovine serum (FBS) (Gemini) and 1% penicillin-streptomycin (DMEM FM). Media were replaced with fresh DMEM FM 24 hrs after plating and every 48 hrs until 80% confluent and then treated with 50% conditioned media with 50% fresh DMEM FM. Twenty-four hours after treatment, DNA content of cell layer lysates was determined. Immunoassays using collected media were performed to measure levels of bone morphogenetic protein 2 (BMP2), osteopontin (OPN), osteoprotegerin (OPG) (R&D Systems), and osteocalcin (OCN) (Thermo Fisher Scientific).

2.4. Preparation of titanium implants and disks

Grit-blasted, acid-etched 3.5 mm long implants x 2.5 mm outer diameter Ti screw implants (SLA, Institut Straumann AG Basel, Switzerland) were machined from grade 4 Ti rod stock as described previously [34]. 15-mm diameter SLA Ti disks were punched from 1-mm thick sheets of grade 2 Ti (Institut Straumann AG) manufactured as previously described [35] and used for *in vitro* studies.

2.5. Experiment design and surgical procedures

Thirty 15-week-old male Zucker Diabetic Sprague Dawley rats (ZDSD) and twenty-eight age-matched male Sprague Dawley rats (SD) (Charles River Laboratories, Wilmington, MA, USA) were used. Twenty-one ZDSD rats developed diabetes, while nine ZDSD rats

did not develop diabetes and were used as the genetic control cohort. Chemically induced models aim to destroy the β -cells and, consequently, the capability to produce insulin. These models simulate the condition of type 1 diabetes. Conversely, the animal model characterized in this study closely replicates a diabetic condition that is similar or almost identical to how type 2 diabetes develops in humans [30,36–38]. Because the ZDSD model is naturally occurring, not all of the ZDSD rat cohort develops a diabetic phenotype, in contrast to chemically induced type 1 diabetes models. This is similar to what is seen in humans, where the majority of diabetic patients that receive implants suffer from varying stages of type 2 disease [30,36–38].

All animal procedures were approved by the Institutional Animal Care and Use Committee at Virginia Commonwealth University. All experiments were carried out following the National Institutes of Health guide for the care and use of laboratory animals. Animals were housed in a single ventilated, solid-bottomed polysulfone cage in an AALAC-accredited animal facility with indoor housing capable of controlling temperature and humidity within species-appropriate ranges and maintaining a 12 h/12 h light/dark cycle.

For all procedures, anesthesia was induced with 5% isoflurane gas inhalation in O_2 and maintained with 2.5% isoflurane gas inhalation in O_2 . Animals were recovered from anesthesia on a water-circulating warming pad before returning to the vivarium. For all surgical procedures, 1 mg/kg of sustained-release Buprenorphine (ZooPharm, Windsor, CO, USA) was administered pre-operatively via subcutaneous injection to provide a minimum of 72 hrs of postoperative analgesia.

2.5.1. Diabetes induction

At 15 weeks of age, all rats were fed a high-fat diet (D12468, Research Diet, New Brunswick, NJ, USA) to induce diabetes [30,31,39,40]. Twenty-one ZDSD rats turned hyperglycemic with nonfasting blood glucose levels higher than 250 mg/dL after 3 weeks. After four weeks, all rats were switched to a standard diet (Purina 5008, LabDiet, St. Louis, MO, USA) and aged for another three weeks before implant surgery. Blood glucose levels were monitored weekly.

2.5.2. Hydrogel loading and implant placements in both hindlimbs

On day 49, diabetic ZDSD rats were randomly assigned to the diabetic empty hydrogel (hydrogel alone) group (Diabetic GEL, N=7 rats, n=14 limbs), the diabetic hydrogel-delivered sema3A group (Diabetic 3A+GEL, N=7 rats, n=14 limbs), or the diabetic locally-injected sema3A group (Diabetic i3A+GEL, N=7 rats, n=14 limbs). Twenty-eight SD rats were randomly assigned to Normal GEL (N=9 rats, n=18 limbs), the Normal 3A+GEL group (N=9 rats, n=18 limbs), and the Normal i3A+GEL (N=10 rats, n=20 limbs).

The implant insertion site was produced by sequentially drilling a defect with increasing diameter dental drill bits (Ø1.0 mm, Ø1.6 mm, Ø2.0 mm, and Ø2.2 mm) to a depth of 3.5 mm in the distal metaphysis of the femur after separating the adjacent muscles and periosteum. 6 µg of sema3A (6 µg/limb) was added to 10.66 µL PEG-DBCO crosslinker [41]. 5.33 µL of PEG-N3 was combined with 16.66 µL of crosslinker mixture by pipetting into the drilled hole simultaneously. After gelation, implants were screwed into the hole immediately, a cover screw applied, and tissues re-approximated and closed with suture and wound clips. The procedure was repeated on the contralateral limb. The mobility of the animals was not affected by implant insertion and loading of the hydrogel. Four weeks later, all rats were euthanized by CO2 inhalation. The nine non-diabetic ZDSD rats were aged until 30 weeks old and used as the genetic control group [30]. Non-diabetic ZDSD rats were randomly assigned to ZDSD (-) GEL (N=3 rats, n=6 limbs), and the ZDSD (-) 3A+GEL (N=3 rats, n=6 limbs), and ZDSD (-) i3A+GEL (N=3 rats, n=6 limbs). Animals were sacrificed four weeks following implant surgery. i3A+GEL groups received local injections of sema3A (6 μg of 100 $\mu g/mL$ sema3A (60 $\mu L)$ in sterile 0.9% NaCl per limb) to both hindlimbs underneath the periosteal layer but above the implant on days 52 and 59. Two diabetic ZDSD rats from the diabetic hydrogel-delivered sema3A group were withdrawn from the study following implantation surgery as they met the humane endpoint.

2.6. Tissue analysis

Parameters for microCT (SkyScan 1173, Bruker, Kontich, Belgium) were identical to the referenced study, except this study used an isotropic voxel size of 15.82 μ m [42]. Adjacent bone formation was also evaluated qualitatively from microCT images by two independent observers blinded to the treatment groups, with the average of the two observers reported. 0: 0%-25% bone around implants; 1: 25%-50% bone around implants; 2: 50%-75% bone around implants; 3: 75%-100% bone around implants. Gap frequency quantification was done by three independent observers blinded to the groups, with the average being reported. Plastic embedded samples were prepared for histology, imaged by a bright field microscope, and evaluated for peri-implant bone growth and bone-to-implant contact (BIC), as described before [42,43]. Removal torque testing was conducted identically as previously described [42]. A torque vs. radian graph was generated for each implant (Supplemental Fig. 1).

Tibial bone marrow from diabetic and normal GEL groups was flushed, pulverized, and RNA or protein was extracted. Total RNA was isolated according to the manufacturer's protocols using TRIzolTM reagent (Thermo Fisher Scientific) and the RNeasy Mini kit (Qiagen, Hilden, Germany) to quantify SEMA3A and GAPDH (Supplemental Table 1). Total protein was extracted from 50 mg of bone powder using MinuteTM Total Protein Extraction Kit for Bone Tissue (Invent Biotechnologies), following the manufacturer's instructions [44]. Sema3A protein production was measured by rat sema3A ELISA kit (MyBioSource) and normalized to the total protein.

Calvarial osteoblasts were isolated using the same protocols as previous studies [45]. Calvarial osteoblasts from the diabetic GEL and SD rats were plated on tissue culture polystyrene surface (TCPS) or SLA surfaces at 10,000 cells/cm² in DMEM FM for 7d. At 7d, cells were incubated with fresh DMEM FM for 24 hrs, and cell-conditioned media were collected for the same immunoassays as Section 2.3, along with Sema3A (LifeSpan Biosciences) and normalized to DNA.

2.7. Statistical analysis

Based on previous studies, eight successful implants are required for each group to ensure implant success in systemic compromised conditions with a 30% mean difference, a 20% variance, and a type I error rate of 0.05 using two-tailed one-way ANOVA analysis to maintain 80% power [45–47]. All statistical analyses are stated in each respective figure legend.

3. Results

3.1. Hydrogel characterization

Force-displacement curves revealed that the hydrogel samples had modest adhesive properties, indicated by the negative force. The area under the curve represented the work done by the plate to stretch the hydrogel to its breaking strain and revealed the cohesive properties of the hydrogel. The tackiness of the hydrogel samples was -3.37 \pm 0.49 N. The gel remained cohesively intact,

and its highly elastic nature allowed it to spring back onto the bottom plate at the point of adhesive failure in approximately half a second (Fig. 1A).

The frequency sweep data revealed that the gel was more solidlike than liquid-like in nature and remained polymerized over the oscillatory frequencies measured. The elastic (G') modulus increased with frequency (0.1-2 Hz) and was larger than the viscous (G") modulus, indicating a stiffer, more solid-like nature. Additionally, the low (2-8°) phase angle supports a firmer, solid-like property, where values between 45 and 90° are more liquid-like. A G'/G" crossover event was not observed between the storage and loss moduli, demonstrating that the hydrogel remained crosslinked after gelation at the frequencies tested. The lack of significant changes in the G' and G" values over the tested time period was an indicator of stable gelation of the hydrogel (Fig. 1B). Oscillatory shear measurements provided the viscosity versus shear rate response of the hydrogel as a measure of shear thinning and ease of injectability. The complex viscosity η^* observed at the lowest frequency tested (0.1 Hz) was 5663.0 \pm 2063.2 Pa-s. The elastic modulus G' was relatively constant while the complex viscosity η^* decreased with angular frequency and increasing shear rate, indicative of shear degradation of the polymer (Fig. 1C). The G'/G" ratio of elasticity was relatively constant and observed to be 10.28 \pm 1.68 at the lowest frequency tested (0.1 Hz) (Fig. 1D). The shear thinning behavior observed verifies the injectability of the hydrogel. Inertia effects were flagged for one sample at two frequencies (15 Hz and 19 Hz), suggesting possible slippage at the plate-sample interface despite using roughened plates and consistent gap force and height (Fig. 1D).

The onset of gelation occurred in under 15 s with minimal changes in total fluorescent intensity and therefore, viscosity, over 5 mins. The glycerol standard exhibited low fluorescence intensity, with detectable fluorescence completely abolished after 3 mins (Fig. 1E). The average horizontal swelling ratio (qt) was determined to be 2.42 \pm 0.14 after 48 h, which is indicative of minimal swelling behavior according to the literature, where slightly swelling hydrogels are defined as having swelling ratios below 8.9 and strongly swelling hydrogels have swelling ratios greater than 16.8 and approaching a ratio of 100 (Fig. 1F). The horizontal swelling ratio of our click hydrogel most closely resembled values reported for polymethacrylic acid (hPMAA) click hydrogels [48] The average vertical swelling after 1 hr was 8.63 \pm 0.63 % (q_t = 0.086 \pm 0.01) for Method 1 and 8.77 \pm 1.75 % $(q_t = 0.19 \pm 0.19)$ for Method 2. After 2 hrs, swelling increased to $8.91 \pm 0.82 \%$ (q_t = 0.09 \pm 0.02) and 21.05 \pm 5.26% (q_t = 0.12 \pm 0.04), respectively, and no additional swelling was observed after 48 hrs (Fig. 1G, and 1H). The ¹H NMR spectra of the copolymer (Fig. 1I) and crosslinker (Fig. 1J) show peaks that correlate with the chemical structure of these hydrogel components.

3.2. ZDSD rats spontaneously developed a diabetic bone phenotype

Rats were characterized as diabetic when their blood glucose was higher than 250 mg/dL for one week [49]. Table 1 shows that all groups started with similar blood glucose levels lower than 250 mg/dL. On implantation surgery day (day 49) and harvest day (day 77), ZDSD rats had higher blood glucose levels (>250 mg/dL) than normal SD rats. After introducing a high-fat diet, the blood glucose of ZDSD rats gradually increased, and 70% of ZDSD rats turned hyperglycemic after three weeks. The control rats maintained normal glycemic values (Fig. 2A). Diabetic rats had lower body weights than normal rats on the day of implantation (Fig. 2B) and at harvest (Fig. 2C). Trabecular bone was analyzed at the metaphysis of the distal femur (Fig. 2D). Diabetes decreased bone volume/total volume (BV/TV) (Fig. 2E), increased total porosity (Fig. 2F), and inhibited trabecular thickness (Fig. 2G) and number (Fig. 2H).

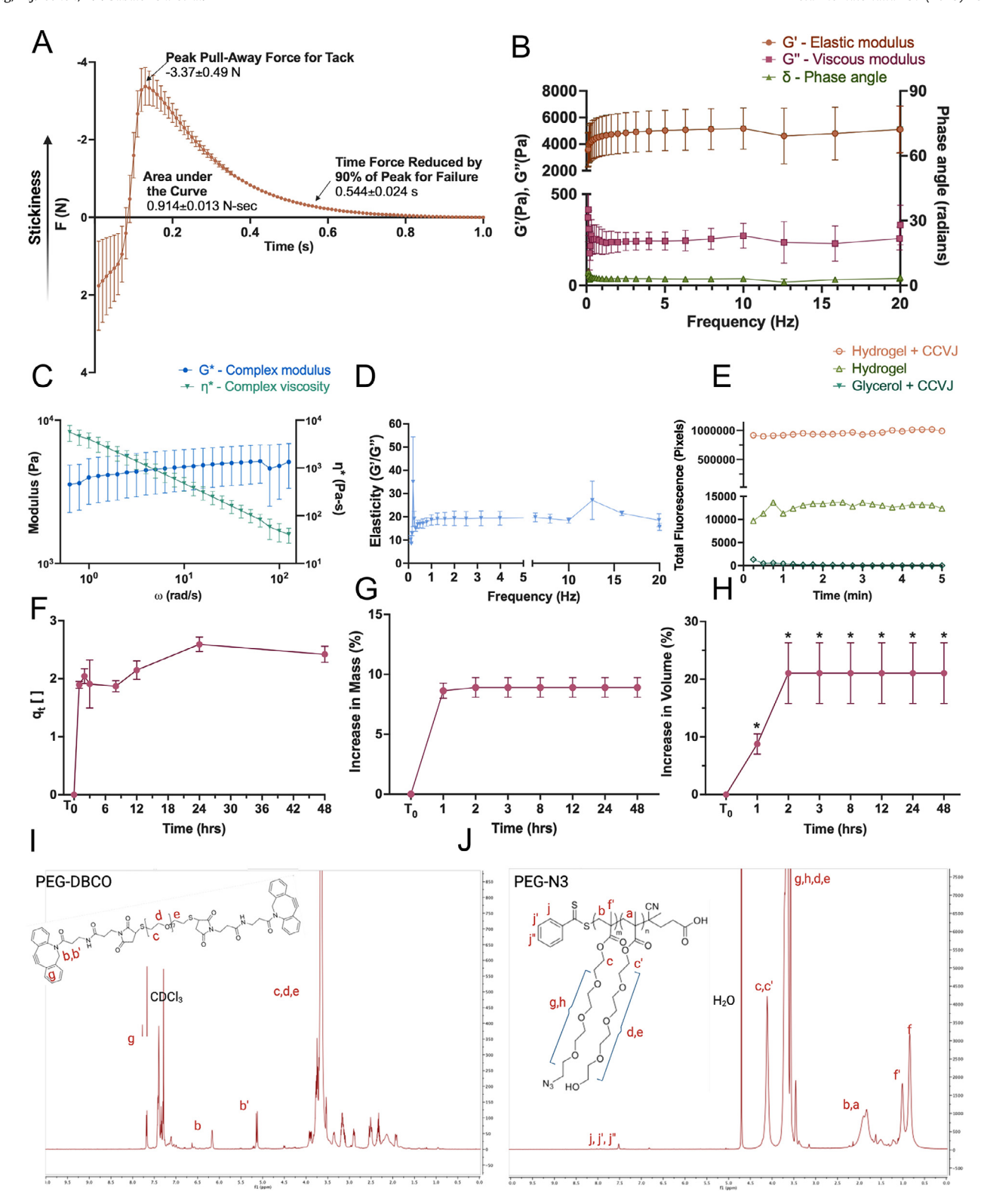


Fig. 1. Physicochemical and rheological properties of rapidly-polymerizing click hydrogels. (A) Squeeze pull-away measurements to assess tackiness of hydrogel samples after 5 min of gelation. The absolute force for tack, time to achieve 90% of force reduction for failure, and area under the curve (N-sec) is indicated to define adhesive and cohesive properties of samples. (B) Frequency sweep performances of the click hydrogel with a fixed strain of 0.5% to determine elastic modulus G', viscous modulus G'', and phase angle at different frequencies (0.05-20 Hz). (C) Frequency sweep performances indicating log values for complex modulus G^* and complex viscosity η^* at different angular frequencies. (D) The ratio of elastic modulus G' to viscous modulus G'' obtained from frequency sweep measurements as a measure of elasticity. (E) Emission intensity values over 5 min of the viscosity-sensitive probe, CCVJ, as a measure of gelation. Total fluorescence intensity is measured by the number of pixels in an image taken by fluorescent microscopy at 497 nm above the set threshold value (>1000 A.U.). (F) Swelling response of click hydrogels when incubated at 37°C in PBS over 48 h, defined by the swelling ratio, qt, or the increase in horizontal surface area over time. (G, H) Vertical swelling capacity of click hydrogels, defined by the percent increase in mass of a hydrogel swelling beyond the constraints of a container, and the measured distance from the T_0 mark that a hydrogel swells within a container after exposure to PBS at 37°C for 48 h. (I, J) Representative images of the T_0 NMR spectra of the individual components of the click hydrogel: the DBCO-functionalized PEG crosslinker (PEG-DBCO) in CDCl₃, and the azide-functionalized RAFT-copolymer (PEG-N3) in D_2 O. Data shown are the means T_0 Section companed to T_0 . Aside from T_0 , no significant differences in swelling were detected when comparing individual time points.

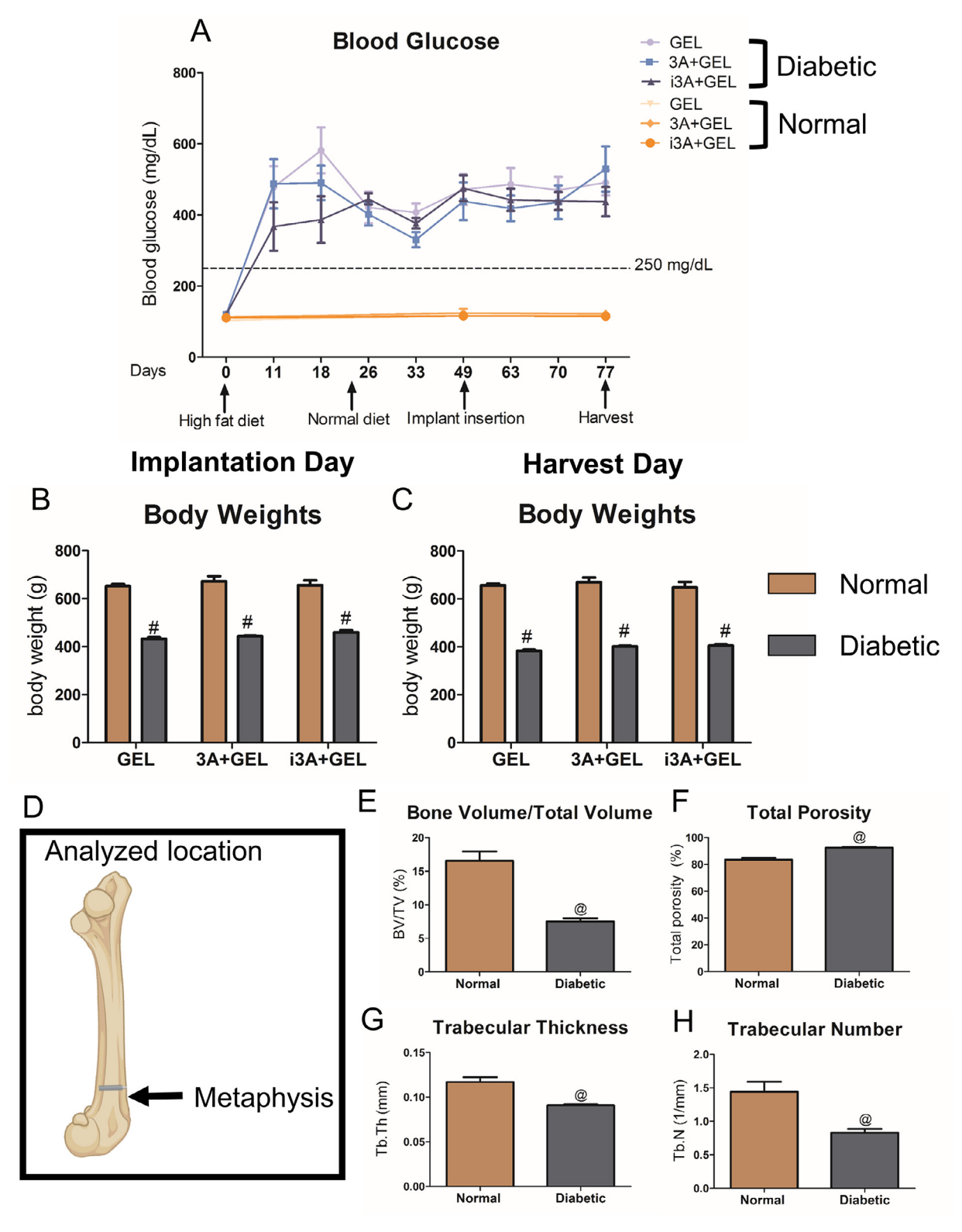


Fig. 2. ZDSD rats spontaneously developed diabetic bone phenotype. 15-week-old male Zucker Diabetic Sprague Dawley rats and age-matched Sprague Dawley rats (normal) were put on a high-fat diet until 70% of ZDSD rats turned diabetic. They were then switched to a regular diet. Both groups of rats were aged for 21 days after ZDSD rats turned diabetic and then were assigned to indicated groups: normal GEL, normal 3A + GEL, normal i3A + GEL, diabetic GEL, diabetic 3A + GEL, and diabetic i3A + GEL, shown in (A). Body weights were measured at indicated time points in normal GEL, normal 3A + GEL, normal i3A + GEL, diabetic GEL, diabetic 3A + GEL, and diabetic i3A + GEL, shown in (A). Body weights were measured on implantation surgery day (B) and animal harvest day (C). The metaphysis of distal femure (D) was analyzed by 3D microCT reconstructions. Trabecular bone formation was evaluated by Bone Volume/Total Volume (E), Total Porosity (F), Trabecular Thickness (G), and Trabecular Number (H). Data shown are the means for each group ± standard error of n=9 for normal GEL and normal 3A + GEL; n=10 for normal i3A + GEL; n=7 for diabetic GEL and diabetic i3A + GEL; and n=5 for diabetic 3A + GEL for body weights and blood glucose level figures. For trabecular bone phenotype characterization, there were n=8 legs per group. Groups with # are statistically different at an $\alpha = 0.05$ by Student's t-test with Bonferroni post-correction compared to normal groups. Groups with * are statistically different at an $\alpha = 0.05$ by one-way ANOVA with Bonferroni post-correction compared to normal groups. Groups with * are significantly different from the normal GEL group at an $\alpha = 0.05$ by unpaired t-test (E–H).

Table 1 Average blood glucose through the course of the study. The high-fat diet was introduced on Day 0. Ti implants were surgically implanted on Day 49. The study concluded 28 days later on Day 77. Data are the means for each group \pm standard error of n=9 for normal GEL and 3A + GEL rats, n=10 for normal i3A + GEL rats, n=7 for diabetic GEL rats and diabetic i3A + GEL rats, n=5 for diabetic 3A + GEL rats. Groups with # are statistically different at an α = 0.05 by student t-test with Bonferroni post-correction compared to normal groups.

Blood Glucose (mg/dL)	Day 0	Day 49	Day 77
Normal GEL	114.50±5.63	117.22±5.73	119.67±8.06
Normal 3A+ GEL	113.00±7.27	113.75±11.37	122.22±5.05
Normal i3A+GEL Diabetic GEL	110.80±3.95	116.3±2.94	115.40±2.48 490.86+35.93#
Diabetic GEL Diabetic 3A+ GEL	122.00±4.07 120.20+2.75	471.71±42.95# 438.6+53.19#	490.86±35.93* 529.40±63.71*
Diabetic i3A+GEL	120.20±2.73 120.29±5.32	475.14±36.34 [#]	437.43±41.35#

3.3. Sema3A released from the hydrogel maintained its bioactivity

Sema3A was gradually released over five days and reached a steady state on day 4 (Fig. 3A). Prior to testing sema3A *in vivo*, we demonstrated its osteogenic capability in MG63. When MG63 cells were treated with hydrogel-released sema3A, DNA content was reduced (Fig. 3B). Osteocalcin (OCN) (Fig. 3C), BMP2 (Fig. 3D), and osteoprotegerin (OPG) (Fig. 3E) were increased; but no change in osteopontin (OPN) (Fig. 3F) was observed. Conditioned media from empty hydrogels (Empty GEL) were compared to conditioned media from sema3A-loaded hydrogels (Sema3A+GEL). In cells treated with Sema3A+GEL media, DNA was reduced (Fig. 3G); there was no difference in OCN (Fig. 3H); and BMP2, OPN, and OPG were increased (Fig. 3I-K) as compared to cells treated with Empty GEL media. The results from these two experiments demonstrated that sema3A released from the click hydrogel maintained its biologic activity.

3.4. Sema3A mitigated the osteopenic bone phenotype in T2DM

Representative microCT images of the trabecular bone phenotype are shown in Fig. 4A-F. Qualitatively, there was less trabecular bone in the diabetic GEL rats than in normal GEL rats (Fig. 4A and D), confirming the quantitative measurements (Fig. 4G-J). In the diabetic rats, sema3A delivered by the hydrogel (labeled as 3A+GEL) increased BV/TV (Fig. 4G), decreased total porosity (Fig. 4H), and increased trabecular thickness (Fig. 4I), but not trabecular number (Fig. 4]), compared to diabetic GEL rats. The effects of diabetes on BV/TV, total porosity, and trabecular thickness (Fig. 4G-I) were eliminated by 3A+GEL but not by sema3A local injection (labeled as i3A+GEL). Both sema3A treatments eliminated the diabetic effect on trabecular number (Fig. 4J). Diabetes did not compromise cortical bone at the metaphysis. There was no change between the normal and diabetic groups in BV/TV, total porosity, and cortical thickness (Fig. 4K-M). However, diabetes decreased the bone perimeter, and only i3A+GEL recovered the difference (Fig. 4N). Diabetes did not affect cortical bone at the middiaphysis (Supplemental Fig. 2A), but sema3A delivered by either hydrogel or local injection increased BV/TV (Supplemental Fig. 2B) and decreased total porosity (Supplemental Fig. 2C). Additionally, 3A+GEL increased mean cross-sectional bone perimeter in diabetic rats (Supplemental Fig. 2D). However, 3A+GEL resulted in lower cortical thickness than GEL in the diabetic rats (Supplemental Fig. 2E). There was no difference in sema3A gene expression (Supplemental Fig. 3A) or protein production (Supplemental Fig. 3B) in extracts of tibial bone from normal and diabetic rats treated with

3.5. Sustained release of sema3A increased marrow BIC and BV/TV

Osseointegration occurred in all groups (Fig. 5A-F). Qualitatively, the attached bone on the titanium implant surfaces was

decreased in diabetic rats compared to normal rats (Supplemental Fig. 4A-F) regardless of sema3A treatment. Quantitatively, total BIC was decreased in diabetic rats and was not modified by sema3A treatments (Fig. 5G). The marrow BIC reduction between normal and diabetic rats remained significant, and 3A+GEL yielded a higher marrow BIC than GEL in the diabetic rats (Fig. 5H). However, i3A+GEL did not restore the marrow BIC to normal. Surprisingly, 3A+GEL decreased the cortical BIC compared to GEL in diabetic animals and exaggerated the difference compared to the normal rats. i3A+GEL ameliorated the difference between normal and diabetic rats in cortical BIC (Fig. 51). Total adjacent bone formation was not compromised by diabetes, indicated by no significance observed in total BV/TV (Fig. 5J). The total adjacent bone was separated into trabecular and cortical bone volume fractions. Diabetes dramatically reduced trabecular bone formation, which 3A+GEL increased. Both sema3A treatments eliminated the diabetic effect on trabecular bone volume (Fig. 5K). Cortical bone formation was not affected by diabetes or sema3A treatment (Fig. 5L). By observing three-dimensional microCT images, diabetes qualitatively reduced adjacent bone formation, and both sema3A treatments ameliorated the bone reduction (Fig. 5M).

3.6. Sema3A increased total BIC regardless of delivery methods

Qualitatively, histology showed less adjacent bone in the T2DM rats than in normal rats (Fig. 6A–F). Total and marrow BIC were dramatically reduced in untreated T2DM animals, and sema3A treatment eliminated the diabetic effect (Fig. 6G, H). Cortical BIC was not affected by diabetes, and diabetic 3A+GEL had lower cortical BIC compared to other diabetic groups (Fig. 6I). Cortical thickness was not affected by diabetes itself, but i3A+GEL treatment did amplify the difference between normal and diabetic rats (Fig. 6J). Total adjacent bone formation was not affected by diabetes but increased in the 3A+GEL group compared to the diabetic GEL group (Fig. 6K).

Gaps were observed by microCT and histology between the cortical bone and implant surfaces in some samples. Gap frequency was greatest for diabetic rats compared to normal rats, and diabetic rats that received sema3A in the metabolically active bone marrow space had the highest gap frequency of all groups (Supplemental Fig. 5A, B).

3.7. Sema3A enhanced the bone mechanical properties in T2DM

Diabetes reduced the maximum torque and torsional stiffness compared to the normal GEL (Fig. 7A and B). Both sema3A treatments mitigated the diabetic effect on maximum torque (Fig. 7C) and torsional stiffness (Fig. 7D). Moreover, sema3A increased the torsional stiffness compared to the diabetic GEL regardless of delivery method (Fig. 7D).

3.8. T2DM cells do not produce more sema3A on SLA surfaces

Calvarial osteoblasts from normal rats produced more sema3A on SLA than TCPS (Fig. 8A), but this was not observed in cultures of osteoblasts from diabetic rats (Fig. 8B). Diabetic osteoblast cultures had less DNA on SLA than TCPS. Sema3A treatment did not affect the DNA amount on TCPS but decreased it on SLA (Fig. 8C). Diabetic osteoblasts produced more OCN on SLA than on TCPS, and sema3A further enhanced the OCN production on SLA (Fig. 8D). Similar data were observed with BMP-2 (Fig. 8E) and OPG production (Fig. 8F). OPN production by diabetic osteoblasts was higher on SLA than TCPS and was not affected by sema3A treatment (Fig. 8G). No difference in VEGF-165 production was observed regardless of surface or treatment (Fig. 8H).

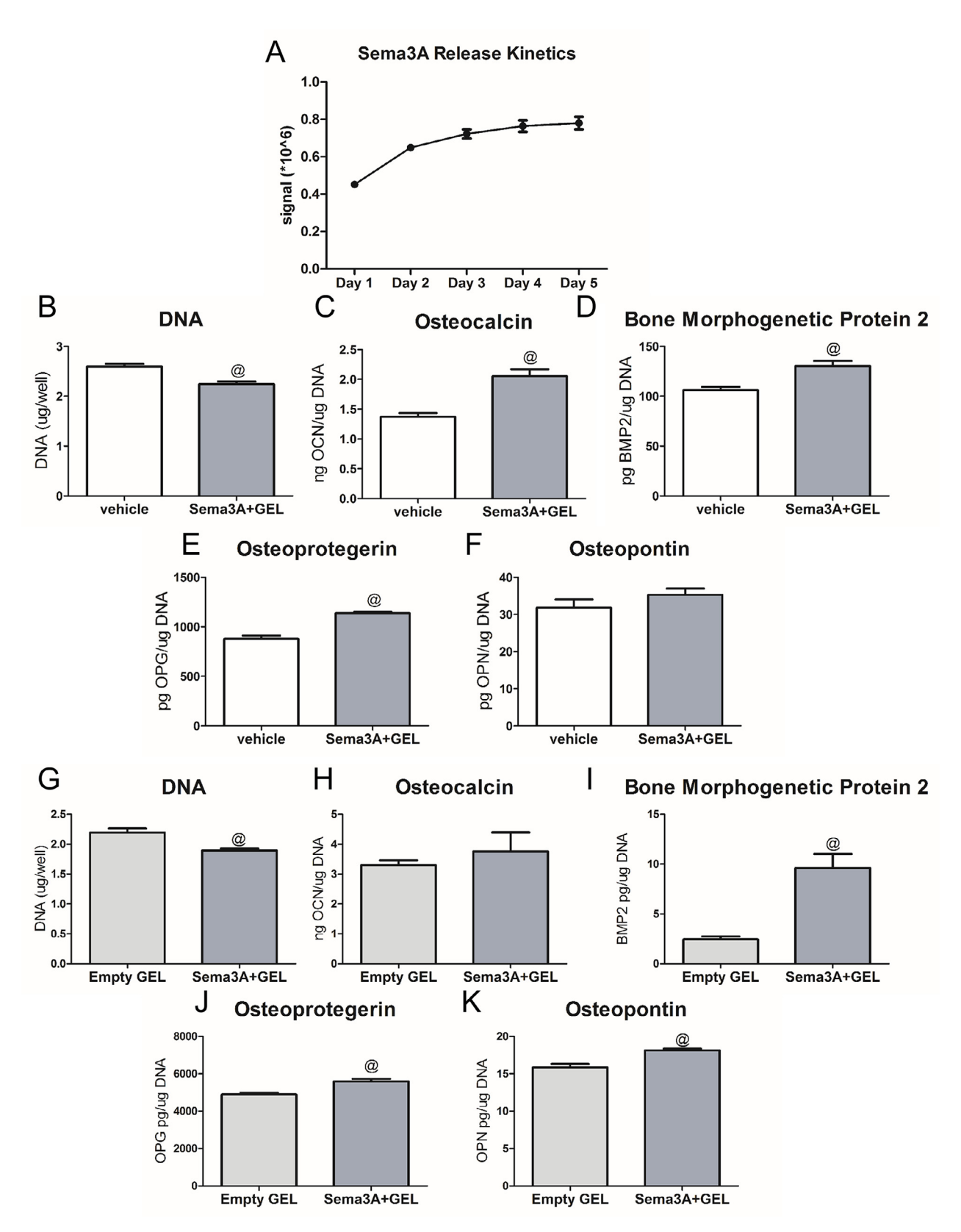
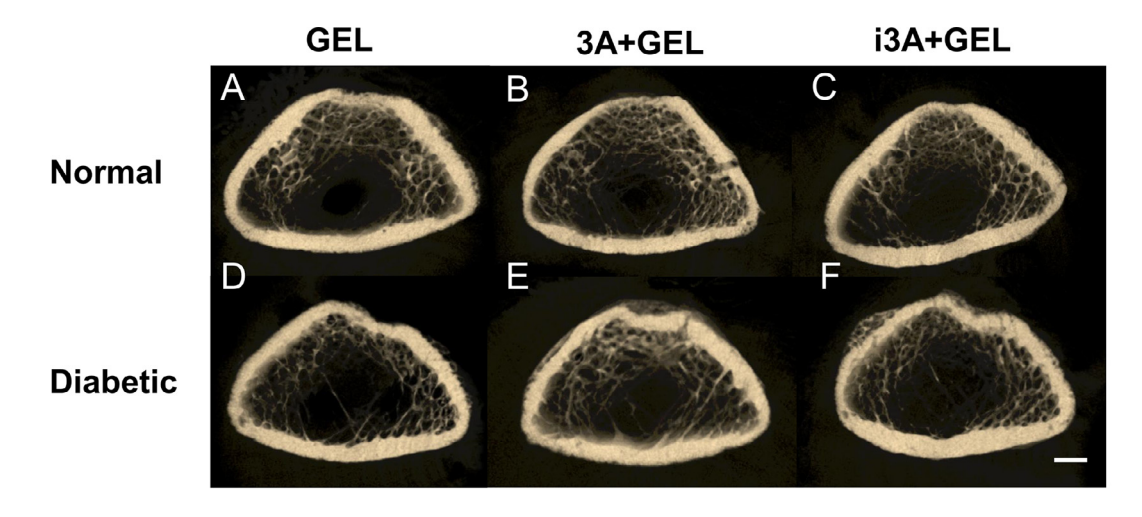


Fig. 3. Sema3A released from hydrogel maintained its bioactivity. Bio-dot assay was conducted over 5 days to determine the release kinetics of sema3A protein from the click hydrogel (A). MG63 cells were cultured on a 24 well plate and treated with vehicle or conditioned media collected from sema3A released from the hydrogel on day 1. The effect of released sema3A on MG63 cell osteoblast differentiation compared to vehicles was assessed by the DNA content (B), production of osteocalcin (C), bone morphogenetic protein 2 (D), osteoprotegerin (E), and osteopontin (F). The comparison to empty hydrogel was assessed by the DNA content (G), osteocalcin production (H), bone morphogenetic protein 2 production (I), osteoprotegerin (J), and osteopontin (K). Data are from a representative experiment and shown as means \pm standard error of n=6 for each group. Groups with "@" were significantly different from vehicle or empty GEL group using unpaired t-test at an $\alpha = 0.05$. Experiments were performed twice to validate the results.



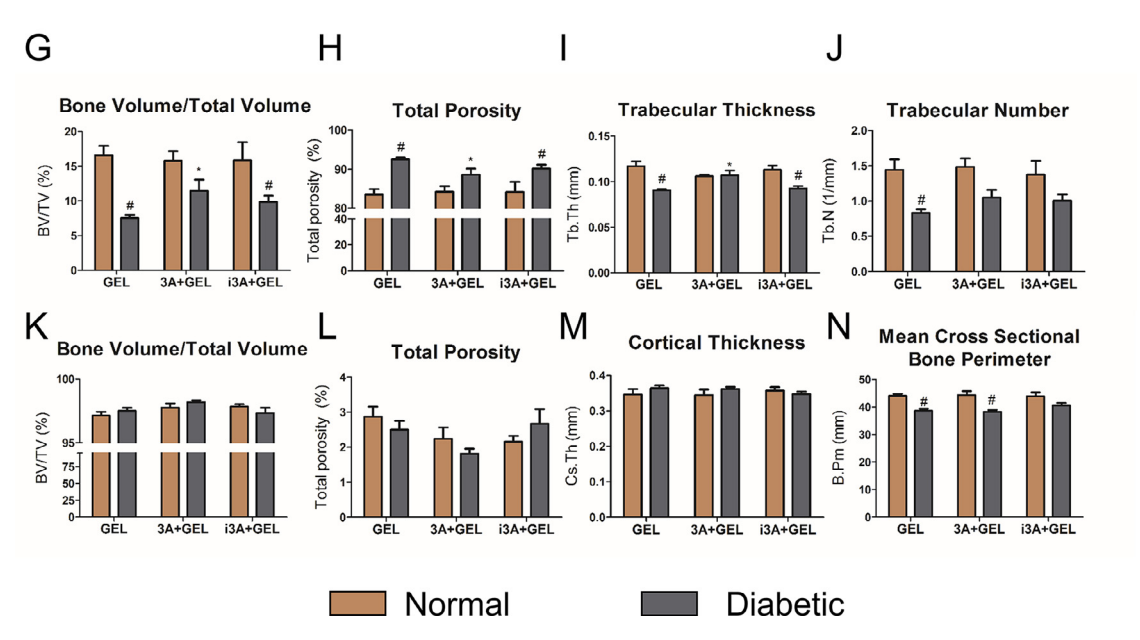


Fig. 4. Sema3A mitigated the osteopenic bone phenotype in T2DM. 15-week-old male Zucker Diabetic Sprague Dawley rats and age-matched Sprague Dawley rats (normal) were put on a high-fat diet until 70% of ZDSD rats turned diabetic and switched to a regular diet. Both rat groups were aged 21 days after ZDSD rats turned diabetic and then assigned to indicated groups: normal GEL, normal 3A + GEL, normal i3A + GEL, diabetic GEL, diabetic 3A + GEL, and diabetic i3A + GEL. After 28 days of osseointegration, femurs were harvested for microCT scanning. The metaphysis of distal femurs was analyzed by microCT reconstruction (A–F). The trabecular bone phenotype was quantified as Bone Volume/Total Volume (G), Total Porosity (H), Trabecular Thickness (I), and Trabecular Number (J). The cortical bone phenotype was quantified as Bone Volume/Total Volume (K), Total Porosity (L), Cortical Thickness (M), and Mean Cross Sectional Bone Perimeter (N). Data shown are the means for each group \pm standard error of n=8 legs/group. Groups with \pm are statistically different at an α = 0.05 by Student's t-test with Bonferroni post-correction compared to normal groups. Groups with \pm are statistically different at an \pm 0.05 by one-way ANOVA with Bonferroni post-correction than the corresponding GEL groups. Scale bar=1 mm

3.9. SD and ZDSD (-) are optimal non-diabetic controls

30% of the ZDSD rats that did not turn diabetic were used as genetic controls (ZDSD (-)). Normal Sprague Dawley rats (SD) and ZDSD (-) had no difference in BV/TV, total porosity, trabecular thickness, and number (Supplemental Fig. 6A–D). Diabetes caused trabecular bone reduction compared to both controls (Supplemental Fig. 6A–D). No difference was observed in the cortical bone phenotype of SD and ZDSD (-) (Supplemental Fig. 6E–H). Diabetic rats increased cortical BV/TV compared to the ZDSD (-) (Supplemental Fig. 6E) and decreased mean cross-sectional bone perimeter compared to both controls (Supplemental Fig. 6G).

ZDSD (-) exhibited similar total BIC and marrow BIC to the SD (Supplemental Fig. 6I and J, and Supplemental Fig. 4A–I). In contrast, they had lower cortical BIC than the SD (Supplemental Fig. 6K). Diabetic rats had comparable levels of all BIC compared to ZDSD (-) (Supplemental Fig. 6I–K). However, when BIC was ana-

lyzed by histology (Supplemental Fig. 4J–L), diabetes reduced all BIC compared to both controls (Supplemental Fig. 6L–N). There was no difference between the control groups regarding total adjacent bone formation, but diabetic rats had less BV/TV than the genetic control (Supplemental Fig. 6O). There was no difference in cortical thickness among the three groups (Supplemental Fig. 6P). There was no significant difference between the SD control rats and the genetic control rats regarding bone phenotype and osseointegration. To validate that the ZDSD genetic control can be used as a non-diabetic control in terms of sema3A treatment, we performed microCT and histologic assessment comparing the genetic control and T2DM (Supplemental Figs. 7 and 8).

4. Discussion

In this study, we proved the use of our injectable click hydrogel as an effective delivery platform for biologics, specifically sema3A,

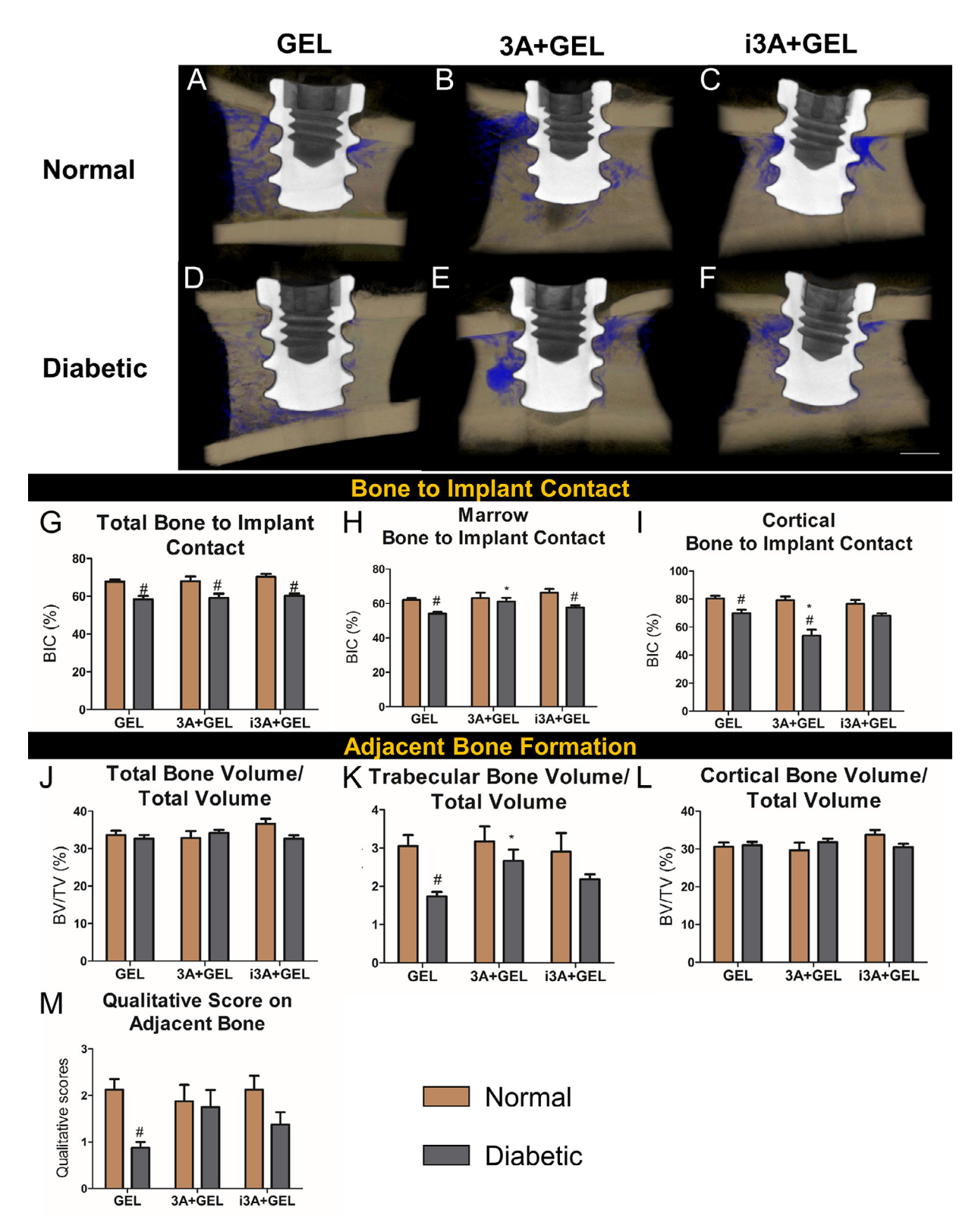


Fig. 5. Sustained release of sema3A increased marrow BIC and BV/TV. Femurs were harvested for microCT analysis (A–F). Tissue colored brown indicates the cortical bone, and purple tissue indicates the trabecular bone. Total Bone to Implant Contact (G) was analyzed further in the subregions: Marrow Bone to Implant Contact (H) and Cortical Bone to Implant Contact (I). Total Bone Volume/Total Volume (J) were analyzed further in the subregions: Trabecular Bone Volume/Total Volume in the bone marrow (K) and Cortical Bone Volume/Total Volume (L). Qualitative Score on Adjacent Bone (M) was evaluated by qualitative observation of adjacent bone around the implant. Data shown are the means for each group \pm standard error of n=8 legs/group. Groups with \pm are statistically different at an α = 0.05 by Student's t-test with Bonferroni post-correction compared to normal groups. Groups with \pm are statistically different at an \pm and \pm and \pm are statistically different at an \pm are st

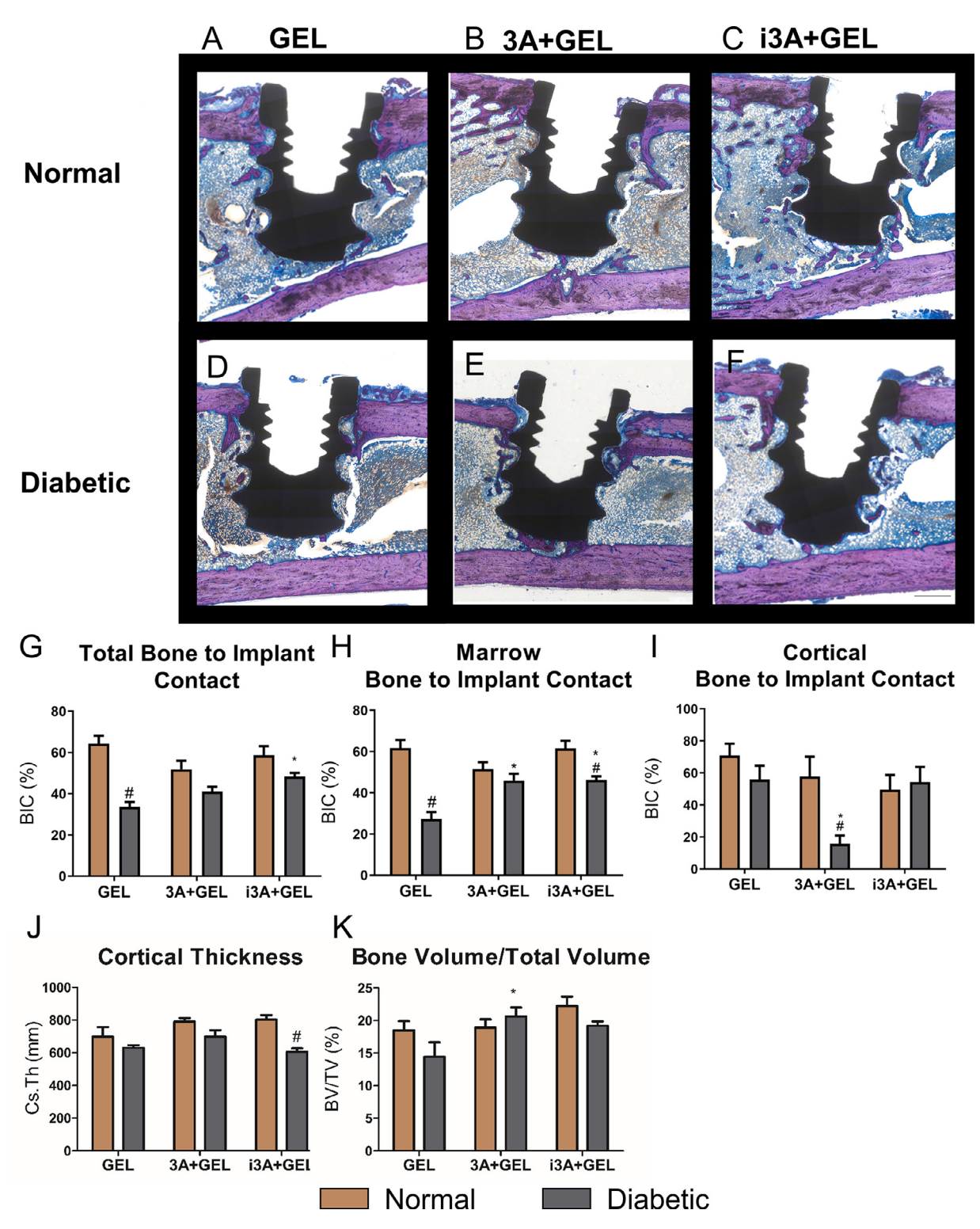


Fig. 6. Sema3A increased total BIC regardless of delivery methods. Isolated femurs were fixed in 10% formalin and then embedded in methyl methacrylate. One ground section was taken from each specimen through the center of each implant in a plane longitudinal to the implant and parallel to the long axis of the bone shaft. All sections were stained with Stevenel's Blue/van Gieson stain and coverslipped (A–F). Osteoid was stained purple and connective tissue was stained blue. Total Bone to Implant Contact (G) was analyzed further into two subregions: Marrow Bone to Implant Contact (H) and Cortical Bone to Implant Contact (I). In addition, Cortical Thickness (J), and Bone Volume/Total Volume (K) were quantified. Data shown are the means for each group \pm standard error of n=6 for normal GEL; n=8 for normal 3A + GEL and normal i3A + GEL; and n=6 for diabetic GEL, diabetic GEL, diabetic i3A + GEL. Groups with # are statistically different at an α = 0.05 by Student's t-test with Bonferroni post-correction compared to normal groups. Groups with * are statistically different at an α = 0.05 by one-way ANOVA with Bonferroni post-correction than the corresponding GEL group. Scare bar= 500 μm.

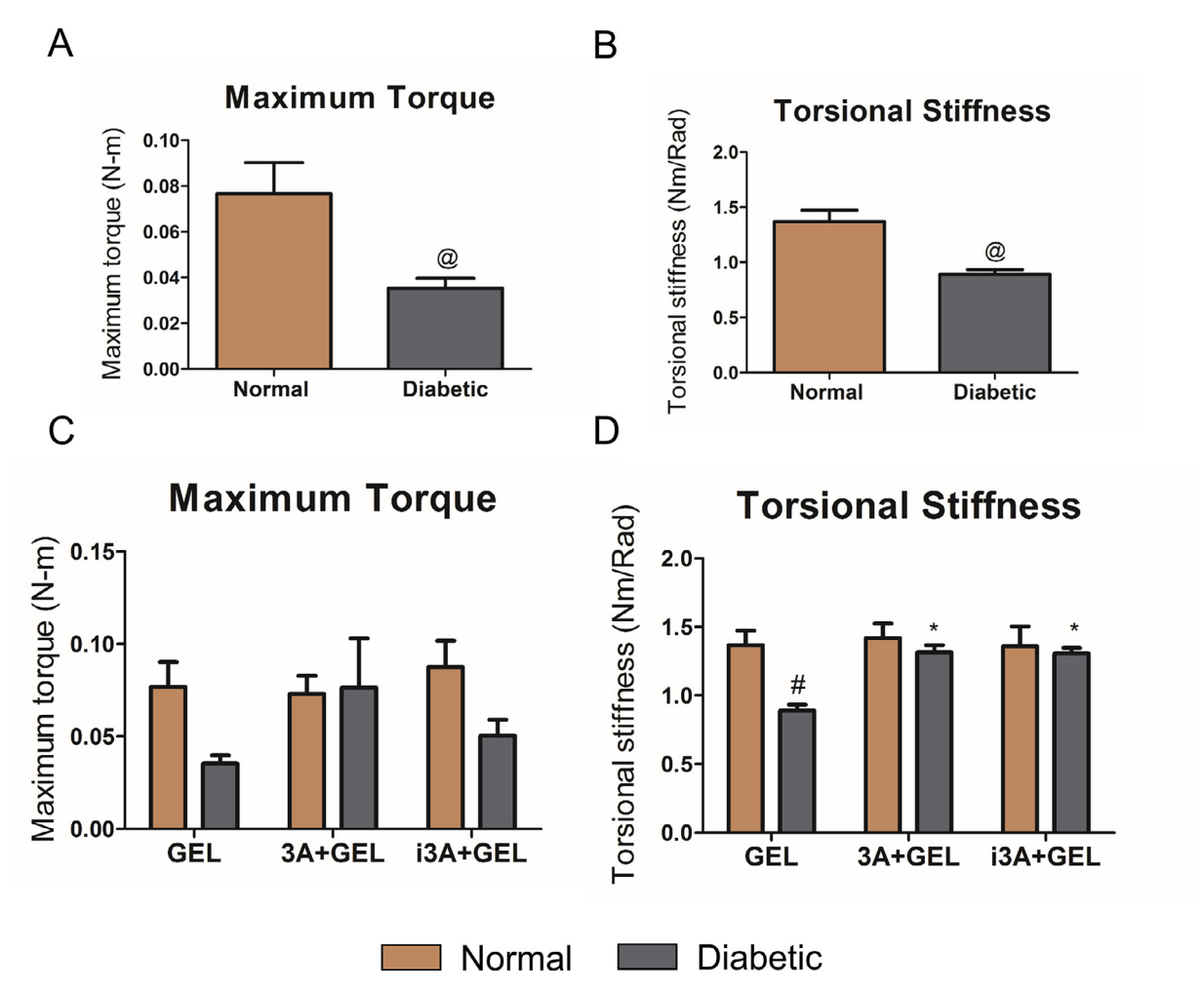


Fig. 7. Sema3A enhanced the bone mechanical properties in T2DM. Maxium Torque (A, C) and torsional stiffness (B, D) were calculated from bilinear curve shown in Supplemental Fig. 1 to evaluate mechanical properties of integrated bone tissues. Data shown are the means for each group \pm standard error of n=6 for normal GEL; n=8 for normal 3A + GEL and normal i3A + GEL, and n=4 for diabetic GEL, diabetic 3A + GEL, and diabetic i3A + GEL. Groups with # are statistically different at an α = 0.05 by Student's t-test with Bonferroni post-correction compared to normal groups. Groups with # are statistically different at an α = 0.05 by Student's t-test with Bonferroni post-correction compared to normal groups. Groups with * are statistically different at an α = 0.05 by one-way ANOVA with Bonferroni post-correction than the corresponding GEL group (C, D).

as a therapeutic to treat impaired osseointegration of implants in compromised patient populations, such as T2DM. As anticipated based on our previous studies examining calvarial bone and underlying dura in weanling mice treated with a similar click hydrogel [25,26], there was no evidence of toxicity to the peri-implant tissues in the present study. In previous studies, no inflammatory cells were observed by histological evaluation at the time of harvest, whereas we did observe some inflammation during the early stages of healing in the peri-implant tissues. It was not connected to the hydrogel, however, suggesting that it was the normal inflammation typically seen when implants are placed *in vivo* [25,48].

Systemic toxicity was not assessed directly in this study. The crosslinker has an amide (peptide bond) that serves as the degradable linkage, degrading at physiological pH in the order of months to years, but has a molecular weight under 6 kDa, facilitating its removal by the kidneys. This crosslinker is attached to the polymer backbone through a monomer that is connected by an ester that degrades in a matter of hours to weeks. All animals survived the surgery and their mobility was unimpaired, indicating that they were healthy, supporting the conclusion that they tolerated the treatment without negative outcomes.

Characterization of the hydrogel revealed attractive mechanical and physicochemical properties, biocompatibility, and rapid *in situ* polymerization without using toxic photo-initiators or organic solvents. Light microscopy and SEM were used to measure the porosity of the hydrogel and we were not able to visualize any pores. These properties demonstrated the broad applicability of our click hydrogel and enabled its potential use in various regenerative and drug delivery applications, especially in challenging implantation environments. Additionally, the production of the individual hydrogel components was found to be easily scalable for a variety of applications.

The rapid *in situ* polymerization of the hydrogel minimizes material migration during gelation while enhancing the mechanical properties such as stiffness without compromising flow properties necessary for injectability. Compared with most conventional hydrogels described in the literature [50,51], our click hydrogel showed substantially less swelling under physiological conditions, especially vertical swelling when confined to the constraints of a container. Reduced swelling in an aqueous environment correlates with improved mechanical properties, reduced slippage from the application site due to minimal temporal changes in shape, and fewer instances of local nerve compression [52]. Additionally, the complex viscosity and G'/G" ratio of elasticity observed with our hydrogel were similar to the viscoelastic properties reported for soft tissues likely contributing to the cytocompatibility of the hy-

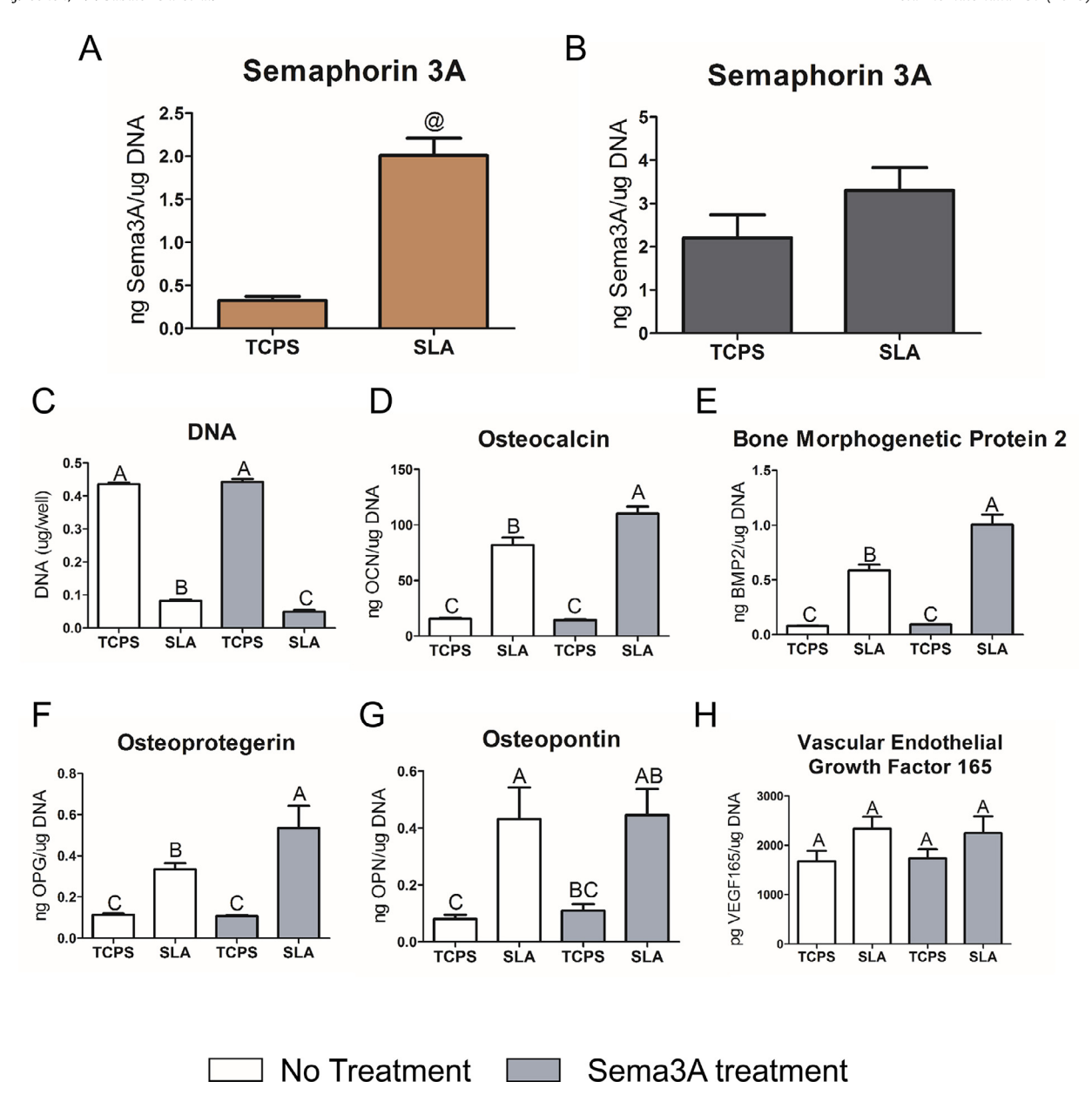


Fig. 8. T2DM cells do not produce more sema3A on SLA surfaces. Primary osteoblasts were isolated from rat frontal and parietal bones and cultured separately on either TCPS or SLA in DMEM full media. Production of sema3A by osteoblasts from Sprague Dawley rats (A) or diabetic rats (B) was graphed. The effect of exogenous sema3A on rat osteoblast differentiation was assessed as a function of DNA content (C). Production of osteocalcin (D), bone morphogenetic protein 2 (E), osteoprotegerin (F), osteopontin (G), and vascular endothelial growth factor 165 (H) was measured by ELISA of the conditioned media. Data are from a representative experiment and shown as means for each group \pm standard error of n=6 individual cultures from pooled rat calvarial osteoblasts. Group with @ are significantly different from the normal GEL group at an α =0.05 by unpaired t-test (A, B). Groups not sharing letters are statistically significant at α =0.05 by one-way ANOVA with Bonferroni post-correction (C-H). Experiments were performed twice to validate the results.

drogel, where its similar viscoelasticity is not expected to alter the local biological and mechanical cues produced *in vivo* [53].

Several studies indicated that diabetes interrupts the process of osseointegration, resulting in poor primary implant loading and subsequent implant failure [54–57]. Surface modification, including the addition of biomimetic roughness, is an efficient way to improve osseointegration by enhancing cellular response to surfaces *in vitro* and increasing bone to implant contact *in vivo* in compromised conditions such as osteoporosis and diabetes [11,43,58]. In our study, we showed that osseointegration was impaired in diabetic rats that did not receive sema3A treatment. In diabetic and osteoporotic phenotypes, animals lose the majority of their trabecular bone, and the bone is almost hollow, which contributes to the bone fragility in human osteoporosis. These results concerning

porosity support our hypothesis that increased porosity in diabetes impacts implant integration.

The grit blasted and acid etched biomimetic surfaces alone could not overcome the detrimental effect of diabetes on osseointegration. Applying a supraphysiologic dose of sema3A in this clinically translatable T2DM model produced greater integration of the implant as measured by microCT and histology and enhanced mechanical properties. It is well established that in T2DM patients, the bone turnover rate is increased 53. In diabetic mice, bone formation and resorption markers were increased compared to non-diabetic control [23]. Sema3A is a well-known osteoprotective factor that works during the bone remodeling phase [59]. The sustained release of sema3A increases the likelihood of maintaining the protein at the needed location in the appropriate time frame

to maximize the effect of sema3A on bone remodeling compared to a burst release strategy. The delivery via this hydrogel platform resulted in increased BIC and adjacent bone formation in the metabolically active bone marrow. Sema3A increased the bone volume fraction and improved the bone quality, indicated by enhanced torsional stiffness, by increasing the ability of the bone to recover under stress. This is important for patients with higher fracture risks due to poor bone quality. The two burst releases of sema3A by injection to the cortical bone around the implants enhanced the cortical BIC, suggesting that a strategy of sustained release of sema3A to both the marrow space and the surrounding cortical bone is critical to maximizing osseointegration.

The effect of sema3A on osseointegration can be attributed to increasing trabecular bone and improving the cellular response to titanium surfaces. We observed that sema3A released by the hydrogel promoted trabecular bone growth and eliminated the differences between normal and diabetic animals, consistent with others' findings [60,61]. Diabetes has been shown to impair cell functions and induce apoptosis. Chronic hyperglycemia alters the response of osteoblasts to parathyroid hormone, leading to decreased differentiation [27]. Our results showed that T2DM osteoblasts still respond to SLA surfaces, indicated by the increase of osteogenic markers. However, these cells did not produce more sema3A. The inability of T2DM osteoblasts to produce more sema3A on the SLA surfaces may be the cause of impaired osseointegration in diabetic rats. The basal level of sema3A in diabetic osteoblasts is higher than in normal rat osteoblasts. We propose that diabetic rats produced more sema3A to compensate for diabetes but could not respond appropriately to the surface signals of the implants in vivo. Moreover, adding sema3A enhanced the surface-induced osteoblast differentiation, perhaps explaining the effect of sema3A in vivo.

The diminished trabecular bone and impaired osseointegration in ZDSD rats could be a result of the complications of vascular and neural dysfunction. Zhang et al. reported that chronic hyperglycemia in ZDSD rats caused vascular and neural dysfunction [62]. Deterioration in vascular response to acetylcholine and the decreased calcitonin gene-related peptide amount in epineurial arterioles of the sciatic nerve was observed in Zucker Diabetic fatty rats [63,64]. Our lab previously demonstrated a lack of sciatic nerve innervation to the bone impaired osseointegration, as well as the importance of vasculogenesis and primary bone remodeling for implant stability [65,66]. Patients with familial dysautonomia have osteoporosis due to the loss of unmyelinated axons, including sensory nerves [60]. Given that nerve-derived sema3A regulates bone remodeling by modulating sensory nerve projections into bone, our sema3A treatment may improve the osseointegration by compensating for the lack of nerve signals or promoting the nerve growth into bones but must be verified in future studies [67].

There were several limitations to our study. Although our data showed that standard and genetic controls could serve as nondiabetic controls, our genetic control was older than other groups with lower sample sizes. The challenge of using a genetic control group as a non-diabetic control is that it is unknown whether these animals will develop diabetes or not. It is impossible to have identically aged animals unless the study begins after 30 weeks of age [30]. However, according to the manufacturer's guidance, conducting any surgeries or treatments at the age of 30 weeks produces other complications such as osteoporosis, neuropathy, nephropathy, cardiovascular deficiency, and fatty liver disease. Another limitation is that the ZDSD T2DM model does not represent obesity-induced T2DM patients, representing a large proportion of the T2DM population. Additionally, we observed some gaps between implants and bone both by microCT and histology. The gap frequency increased in diabetic rats, especially when sema3A was delivered to the bone marrow. Further studies are necessary to investigate this observation.

5. Conclusions

Our study has identified that trabecular bone formation and osseointegration were decreased in a clinically translatable type 2 diabetic rat model. Furthermore, both the sustainable and burst release of sema3A at the implant site was shown to restore diabetic-impaired osseointegration and halt the progression of the trabecular bone resorption. These *in vivo* results were supported by *in vitro* sema3A treatment studies showing that sema3A may increase the peri-implant bone growth by improving the osteoblastic differentiation on SLA disks.

We are the first to demonstrate sustained release of sema3A to the implant site using a rapidly polymerizing click hydrogel as a drug delivery system. This strategy allowed rapid encapsulation of sema3A at the local delivery site while retaining the bioactivity of the protein. This method has important implications for future applications in regenerative medicine. Importantly, we demonstrated the therapeutic potential of sema3A on bone healing and regeneration in a clinically translatable T2DM rodent model and reported the potential mechanisms of its effect both *in vivo* and *in vitro*.

Disclosures

The titanium surfaces and implants materials for this study were supported by Institute Straumann AG, Basel, Switzerland.

The click hydrogel carrier is licensed by Virginia Commonwealth University to Pascal Medical Corporation, Richmond, Virginia.

BDB is a co-founded of Pascal Medical and has equity in the company.

DJC is a consultant for Pascal Medical.

Declaration of Competing Interest

The authors declare that they have no known competing financial interests or personal relationships that could have appeared to influence the work reported in this paper.

CRediT authorship contribution statement

Jingyao Deng: Visualization, Writing – original draft, Data curation, Formal analysis. David J. Cohen: Visualization, Writing – original draft, Data curation, Formal analysis, Writing – review & editing. Eleanor L. Sabalewski: Data curation. Christine Van Duyn: Visualization, Data curation, Formal analysis, Writing – review & editing. D. Scott Wilson: Formal analysis, Data curation, Writing – review & editing. Zvi Schwartz: Visualization, Data curation, Writing – review & editing. Barbara D. Boyan: Data curation, Writing – review & editing.

Acknowledgments

Institut Straumann AG (Basel, Switzerland) provided microrough and hydrophobic titanium implants and implant SLA surfaces, as well as support for this study. All animals from these studies were a gift from Charles River Laboratories. Additional support was provided by the National Institute of Arthritis and Musculoskeletal and Skin Disease of the National Institute of Health under Award Number R01AR072500. The content is solely the authors' responsibility and does not necessarily represent the official views of the National Institutes of Health. The authors thank Pascal Medical Corporation, the Virginia Biosciences Health Research Corporation, and the Joan and Morgan Massey Foundation for their generous support of our research on click hydrogels. The study is in partial fulfillment of the Ph.D. degree for Jingyao Deng.

Supplementary materials

Supplementary material associated with this article can be found, in the online version, at doi:10.1016/j.actbio.2022.11.030.

References

- [1] S. Wild, G. Roglic, A. Green, R. Sicree, H. King, Estimates for the year 2000 and projections for 2030, World Health 27 (5) (2004) 1047-1053.
- [2] M. Deepa, M. Grace, B. Binukumar, R. Pradeepa, S. Roopa, H.M. Khan, Z. Fatmi, M.M. Kadir, I. Naeem, V.S. Ajay, R.M. Anjana, M.K. Ali, D. Prabhakaran, et al., High burden of prediabetes and diabetes in three large cities in South Asia: The Center for cArdio-metabolic Risk Reduction in South Asia (CARRS) Study, Diabetes Res. Clin. Pract. 110 (2) (2015) 172-182.
- [3] I. Turkyilmaz, One-year clinical outcome of dental implants placed in patients with type 2 diabetes mellitus: a case series, Implant Dent. 19 (4) (2010) 323-329
- [4] S. Dowell, T.W. Oates, M. Robinson, Implant success in people with type 2 diabetes mellitus with varying glycemic control: a pilot study, J. Am. Dent. Assoc. 138 (3) (2007) 355-361.
- [5] R. Dubey, D. Gupta, A. Singh, Dental implant survival in diabetic patients; review and recommendations, Natl. J. Maxillofac. Surg. 4 (2) (2013) 142.
- [6] G. Pavya, N.A. Babu, Effect of diabetes in osseointegration of dental implant -a review, Biomed. Pharmacol. J. 8SE (2015) 353-358.
- [7] T.W. Oates, S. Dowell, M. Robinson, C.A. McMahan, Glycemic control and implant stabilization in type 2 diabetes mellitus, J. Dent. Res. 88 (4) (2009) 367-371
- [8] G. Tawil, R. Younan, P. Azar, G. Sleilati, Conventional and advanced implant treatment in the type II diabetic patient: surgical protocol and long-term clinical results, Int. J. Oral Maxillofac. Implants 23 (4) (2008) 744-752.
- [9] M. Peled, L. Ardekian, N. Tagger-Green, Z. Gutmacher, E.E. Machtei, Dental implants in patients with type 2 diabetes mellitus: a clinical study, Implant Dent. 12 (2) (2003) 116-122.
- [10] B.D. Boyan, A. Cheng, R. Olivares-Navarrete, Z. Schwartz, Implant surface design regulates mesenchymal stem cell differentiation and maturation, Adv. Dent. Res. 28 (1) (2016) 10-17.
- [11] B.D. Boyan, E.M. Lotz, Z. Schwartz, Roughness and hydrophilicity as osteogenic biomimetic surface properties, Tissue Eng. Part A 23 (23-24) (2017) 1479-1489
- [12] A. Wennerberg, T. Albrektsson, On implant surfaces: a review of current knowledge and opinions, Int. J. Oral Maxillofac. Implants 25 (1) (2009) 63-74.
- [13] Z. Schwartz, E.M. Lotz, M.B. Berger, B.D. Boyan, The effect of substrate microtopography on osteointegration of titanium implants, in: Comprehensive Biomaterials II, 7, Elsevier, 2017, pp. 429-443.
- [14] S.L. Hyzy, R. Olivares-Navarrete, S. Ortman, B.D. Boyan, Z. Schwartz, Bone morphogenetic protein 2 alters osteogenesis and anti-inflammatory profiles of mesenchymal stem cells induced by microtextured titanium in vitro, Tissue Eng. Part A 23 (19-20) (2017) 1132-1141.
- [15] R. Olivares-Navarrete, S.L. Hyzy, D.L. Hutton, C.P. Erdman, M. Wieland, B.D. Boyan, Z. Schwartz, Direct and indirect effects of microstructured titanium substrates on the induction of mesenchymal stem cell differentiation towards the osteoblast lineage, Biomaterials 31 (10) (2010) 2728-2735 [Internet]Available from:, doi:10.1016/j.biomaterials.2009.12.029.
- [16] E.M. Lotz, R. Olivares-Navarrete, S.L. Hyzy, S. Berner, Z. Schwartz, B.D. Boyan, Comparable responses of osteoblast lineage cells to microstructured hydrophilic titanium-zirconium and microstructured hydrophilic titanium, Clin. Oral Implants Res. 28 (7) (2017) e51-e59.
- [17] L. Verlinden, D. Vanderschueren, A. Verstuyf, Semaphorin signaling in bone, Mol. Cell. Endocrinol. 432 (2016) 66-74.
- [18] X. Chen, Z. Wang, N. Duan, G. Zhu, E.M. Schwarz, C. Xie, Osteoblast-osteoclast interactions, Connect. Tissue Res. 59 (2) (2018) 99-107.
- [19] T. Negishi-Koga, H. Takayanagi, Bone cell communication factors and semaphorins, Bonekey Rep. 1 (2012) 183 Sep 19.
- [20] B.J. Kim, J.M. Koh, Coupling factors involved in preserving bone balance, Cell. Mol. Life Sci. 76 (2018) 1243-1253.
- [21] M. Hayashi, T. Nakashima, M. Taniguchi, T. Kodama, A. Kumanogoh, H. Takayanagi, Osteoprotection by semaphorin 3A, Nature 485 (7396) (2012)
- [22] Q. Qiao, X. Xu, Y. Song, S. Song, W. Zhu, F. Li, Semaphorin 3A promotes osteogenic differentiation of BMSC from type 2 diabetes mellitus rats, J. Mol. Histol. 49 (4) (2018) 369-376.
- [23] L. Zhang, L. Zheng, C. Li, Z. Wang, S. Li, L. Xu, Sema3a as a novel therapeutic option for high glucose-suppressed osteogenic differentiation in diabetic osteopathy, Front. Endocrinol. 10 (August) (2019) 1–11 (Lausanne).
- [24] E.M. Lotz, M.B. Berger, B.D. Boyan, Z. Schwartz, Regulation of mesenchymal stem cell differentiation on microstructured titanium surfaces by semaphorin 3A, Bone 134 (January) (2020) 115260 [Internet] Available from:, doi:10.1016/j. bone.2020.115260.
- [25] C.D. Hermann, DS.L Wilson, A. Kelsey, X. Ning, R. Olivares-Navarrete, J.K. Williams, RE. Guldberg, N. Murthy, Z. Schwartz, B.D. Boyan, Rapidly polymerizing injectable click hydrogel therapy to delay bone growth in a murine re-synostosis model, Biomaterials 35 (36) (2014) 9698–9708 [Internet]Available from:, doi:10.1016/j.biomaterials.2014.07.065.
- [26] SL. Hyzy, I. Kajan, D.S. Wilson, K.A. Lawrence, D. Mason, J.K. Williams, R. Olivares-Navarrete, D.J. Cohen, Z. Schwartz, B.D. Boyan, Inhibition of angiogenesis

- impairs bone healing in an in vivo murine rapid resynostosis model, J. Biomed. Mater. Res. A 105 (10) (2017) 2742-2749.
- [27] M. Zhang, X.Y. Lv, J. Li, Z.G. Xu, L. Chen, The characterization of high-fat diet and multiple low-dose streptozotocin induced type 2 diabetes rat model, Exp. Diabetes Res. 2008 (2008) 704045.
- [28] K. Srinivasan, B. Viswanad, L. Asrat, C.L. Kaul, P. Ramarao, Combination of high--fat diet-fed and low-dose streptozotocin-treated rat: A model for type 2 diabetes and pharmacological screening, Pharmacol. Res. 52 (4) (2005) 313-320.
- B. Wang, P. Chandrasekera, J. Pippin, Leptin- and leptin receptor-deficient rodent models: relevance for human type 2 diabetes, Curr. Diabetes Rev. 10 (2) (2014) 131-145.
- [30] S. Reinwald, R.G. Peterson, M.R. Allen, D.B. Burr, Skeletal changes associated with the onset of type 2 diabetes in the ZDF and ZDSD rodent models, Am. I.
- Physiol. Endocrinol. Metab. 296 (4) (2009) 765–774. [31] E.P. Davidson, L.J. Coppey, A. Holmes, S. Lupachyk, B.L. Dake, C.L. Oltman, R.G. Peterson, M.A. Yorek, Characterization of diabetic neuropathy in the zucker diabetic sprague-dawley rat: a new animal model for type 2 diabetes, Diabetes Res. 2014 (2014) 1-7
- [32] G. Sun, G. Zhang, C.V. Jackson, Y.X. Wang (Jim), Zucker Diabetic Sprague Dawley (ZDSD) rat, a spontaneously diabetic rat model develops cardiac dysfunction and compromised cardiac reserve, Cardiol. Res. Cardiovasc. Med. 3 (1) (2018) 000033, doi:10.29011/CRCM-133.
- [33] A.C. Chlebowski, G.E. Kisby, Protocol for high-throughput screening of neural cell or brain tissue protein using a Dot-Blot technique with near-infrared imaging, STAR Proto. 1 (2) (2020) 100054.
- [34] E.M. Lotz, D.J. Cohen, Z. Schwartz, B.D. Boyan, Titanium implant surface properties enhance osseointegration in ovariectomy induced osteoporotic rats without pharmacologic intervention, Clin. Oral Implants Res. 31 (4) (2020) 374-387 Apr 1.
- [35] E. Lotz, M. Berger, B. Boyan, Z. Schwartz, Regulation of mesenchymal stem cell differentiation on microstructured titanium surfaces by semaphorin 3A, Bone 134 (January) (2020) 115260.
- S. Choy, W. de Winter, M.O. Karlsson, M.C. Kjellsson, Modeling the disease progression from healthy to overt diabetes in ZDSD rats, AAPS J. 18 (5) (2016) 1203-1212.
- [37] D. Chen, M.W. Wang, Development and application of rodent models for type 2 diabetes, Diabetes Obes. Metab. 7 (4) (2005) 307-317.
- [38] R.G. Peterson, C.V. Jackson, K. Zimmerman, W. de Winter, N. Huebert, M.K. Hansen, Characterization of the ZDSD rat: a translational model for the study of metabolic syndrome and type 2 diabetes, J. Diabetes Res. 2015 (2015) 87-108.
- [39] N. Bhamb, L.E.A. Kanim, R.C. Maldonado, T.J. Nelson, K. Salehi, J.D. Glaeser, M.F. Metzger, The impact of type 2 diabetes on bone metabolism and growth after spinal fusion, Spine J. 19 (6) (2019) 1085-1093.
- K.M.H. Gallant, M.A. Gallant, D.M. Brown, A.Y. Sato, J.N. Williams, D.B. Burr, Raloxifene prevents skeletal fragility in adult female zucker diabetic spraguedawley rats, PLoS One 9 (9) (2014) 1-7.
- [41] X. Xu, K. Fang, L. Wang, X. Liu, Y. Zhou, Y. Song, T. Ogasawara, Local application of semaphorin 3A combined with adipose-derived stem cell sheet and anorganic bovine bone granules enhances bone regeneration in type 2 diabetes mellitus rats, Stem Cells Int 2019 (2019) 2506463.
- [42] J. Deng, D.J. Cohen, J. Redden, M.J. McClure, B.D. Boyan, Z. Schwartz, Differential effects of neurectomy and botox-induced muscle paralysis on bone phenotype and titanium implant osseointegration, Bone 153 (March) (2021) 116145.
- [43] E.M. Lotz, D.J. Cohen, Z. Schwartz, B.D. Boyan, Titanium implant surface properties enhance osseointegration in ovariectomy induced osteoporotic rats without pharmacologic intervention, Clin. Oral Implants Res. 31 (4) (2020) 374-387.
- [44] H. Ren, Z. Wang, J. Xu, J. Chen, J. Lan, The impact of frizzled-9 on dental implant osseointegration in hyperlipidemic rats, J. Hard Tissue Biol. 29 (1) (2020)
- [45] E.M. Lotz, D.J. Cohen, R.A. Ellis, J.S. Wayne, Z. Schwartz, B.D. Boyan, Ibandronate treatment before and after implant insertion impairs osseointegration in aged rats with ovariectomy induced osteoporosis, JBMR Plus 3 (7) (2019) e10184.
- J. McMillan, R.C. Kinney, D.M. Ranly, S. Fatehi-Sedeh, Z. Schwartz, B.D. Boyan, Osteoinductivity of demineralized bone matrix in immunocompromised mice and rats is decreased by ovariectomy and restored by estrogen replacement, Bone 40 (1) (2007) 111-121.
- [47] R. Olivares-Navarrete, A.L. Raines, S.L. Hyzy, J.H. Park, D.L. Hutton, D.L. Cochran, B.D. Boyan, Z. Schwartz, Osteoblast maturation and new bone formation in response to titanium implant surface features are reduced with age, J. Bone Miner. Res. 27 (8) (2012) 1773-1783.
- [48] J. Claus, A. Brietzke, C. Lehnert, S. Oschatz, N. Grabow, U. Kragl, Swelling characteristics and biocompatibility of ionic liquid based hydrogels for biomedical applications, PLoS One 15 (4) (2020) 1–16.
- [49] R.J. Fajardo, L. Karim, V.I. Calley, M.L. Bouxsein, A review of rodent models of type 2 diabetic skeletal fragility, J. Bone Miner. Res. 29 (5) (2014) 1025-1040.
- [50] H. Kamata, X. Li, U.I. Chung, T. Sakai, Design of hydrogels for biomedical applications, Adv. Healthc. Mater. 4 (16) (2015) 2360–2374.

 [51] S.H. Aswathy, U. Narendrakumar, I. Manjubala, Commercial hydrogels for
- biomedical applications, Heliyon 6 (4) (2020) e03719.
- [52] L. Saunders, P.X. Ma, Self-healing supramolecular hydrogels for tissue engineering applications, Macromol. Biosci. 19 (1) (2019) 1-11.
- [53] H. Hasegawa, S. Ozawa, K. Hashimoto, T. Takeichi, T. Ogawa, Type 2 diabetes impairs implant osseointegration capacity in rats, Int. J. Oral Maxillofac. Implants 23 (2) (2008) 237-23746.

- [54] Ding X., Yang L., Hu Y., Yu J., Tang Y., Luo D., Zheng L. Effect of local application of biphosphonates on improving peri-implant osseointegration in type-2 diabetic osteoporosis. 2019;11(9):5417–37.
- [55] T. Jia, W.Y. nan, J. Zhang, X. Hao, D. Zhang, X. Xu, Cinaciguat in combination with insulin induces a favorable effect on implant osseointegration in type 2 diabetic rats, Biomed.Pharmacother. 118 (44) (2019) 109216.
- [56] J. Zhang, M. Shirai, R. Yamamoto, Y. Yamakoshi, S. Oida, C. Ohkubo, J. Zeng, Effect of nerve growth factor on osseointegration of titanium implants in type 2 diabetic rats, Int. J. Oral Maxillofac. Implants (2016) 1189–1194.
- [57] W. Zhou, S. Tangl, K.M. Reich, F. Kirchweger, Z. Liu, W. Zechner, C. Ulm, X. Rausch-Fan, The influence of type 2 diabetes mellitus on the osseointegration of titanium implants with different surface modifications-A histomorphometric study in high-fat diet/low-dose streptozotocin-treated rats, Implant Dent. 28 (1) (2019) 11–19.
- [58] F. Sassi, I. Buondonno, C. Luppi, E. Spertino, E. Stratta, M. Di Stefano, M. Ravazzoli, G. Isaia, M. Trento, P. Passera, M. Porta, G.C. Isaia, P. D'Amelio, Type 2 diabetes affects bone cells precursors and bone turnover, BMC Endocr. Disord. 18 (1) (2018) 1–8.
- [59] S. Kenan, Ö.D. Onur, S. Solakoğlu, T. Kotil, M. Ramazanoğlu, H.H. Çelik, M. Ocak, B. Uzuner, E. Fıratlı, Investigation of the effects of semaphorin 3A on new bone formation in a rat calvarial defect model, J. Cranio-Maxillofac. Surg. 47 (3) (2019) 473–483 Mar 1.
- [60] T. Fukuda, S. Takeda, R. Xu, H. Ochi, S. Sunamura, T. Sato, S. Shibata, Y. Yoshida, Z. Gu, A. Kimura, C. Ma, C. Xu, W. Bando, K. Fujita, K. Shinomiya, T. Hirai, Y. Asou, M. Enomoto, H. Okano, A. Okawa, H. Itoh, Sema3A regulates bonemass accrual through sensory innervations, Nature 497 (7450) (2013) 490–493.

- [61] A.K. Picke, G. Campbell, N. Napoli, L.C. Hofbauer, M. Rauner, Update on the impact of type 2 diabetes mellitus on bone metabolism and material properties, Endocr. Connect, 8 (3) (2019) R55–R70.
- [62] C.L. Oltman, L.J. Coppey, J.S. Gellett, E.P. Davidson, D.D. Lund, MA. Yorek, Progression of vascular and neural dysfunction in sciatic nerves of Zucker diabetic fatty and Zucker rats, Am. J. Physiol. Endocrinol. Metab. 289 (2005) 113–122 (1 52-1).
- [63] L.J. Coppey, J.S. Gellett, E.P. Davidson, J.A. Dunlap, M.A. Yorek, Changes in endoneurial blood flow, motor nerve conduction velocity and vascular relaxation of epineurial arterioles of the sciatic nerve in ZDF-obese diabetic rats, Diabetes Metab. Res. Rev. 18 (1) (2002) 49–56.
- [64] A.L. Raines, M.B. Berger, N. Patel, S.L. Hyzy, B.D. Boyan, Z. Schwartz, VEGF-A regulates angiogenesis during osseointegration of Ti implants via paracrine/autocrine regulation of osteoblast response to hierarchical microstructure of the surface, J. Biomed. Mater. Res. A 107 (2) (2019) 423–433.
- [65] M. Marenzana, T.R. Arnett, The key role of the blood supply to bone, Bone Res. 1 (2013) 203–215.
- [66] C. Maayan, E. Bar-On, A.J. Foldes, B. Gesundheit, R.D. Pollak, Bone mineral density and metabolism in familial dysautonomia, Osteoporos. Int. 13 (5) (2002) 429–433
- [67] P. Saeedi, I. Petersohn, P. Salpea, B. Malanda, S. Karuranga, N. Unwin, S. Colagiuri, L. Guariguata, A.A. Motala, K. Ogurtsova, J.E. Shaw, D. Bright, R. Williams, Global and regional diabetes prevalence estimates for 2019 and projections for 2030 and 2045: results from the International Diabetes Federation Diabetes Atlas, 9th edition, Diabetes Res. Clin. Pract. 157 (2019) 107843.